Chinese Chemical Letters 33 (2022) 5180–5183

Contents lists available at ScienceDirect

Chinese Chemical Letters

journal homepage: www.elsevier.com/locate/cclet

Rapidly SO_2-responsive vesicles with intrinsic fluorescent indicators for membrane structure evolution

Yuan Zhu[a,b], Yuanmei Hu[a,b], Juanmei Zeng[a,b], Chaoxiang Chen[a,b], Shunhua Li[a,b,*], Yunbao Jiang[a,b]

[a] Department of Chemistry and the MOE Key Laboratory of Spectrochemical Analysis & Instrumentation, College of Chemistry and Chemical Engineering, Xiamen University, Xiamen 361005, China
[b] Xiamen Key Laboratory of Analytical Molecular Nanotechnology, Xiamen University, Xiamen 361005, China

ARTICLE INFO

Article history:
Received 26 September 2021
Revised 9 January 2022
Accepted 2 February 2022
Available online 6 February 2022

Keywords:
Sulfur dioxide
Vesicles
Fluorescence
Self-assembly
Membrane probes

ABSTRACT

Stimuli-responsive vesicles (SRVs) have been widely exploited as smart nanocarriers for biomedical applications. Herein, high-performance SO_2-responsive nanovesicles were reported to exemplify a new mode of SRVs. Structurally, the sensory vesicles were based on amphiphilic hydrogen-bonded (HB) polymers which can be facilely fabricated *via* modular self-assembly. The HB polymers are designed to consist of a melamine-barbituric acid HB skeleton with pendant anthracene fluorophores and amphiphilic side chains. Upon stimulation with increasing amount of SO_2, the vesicles in aqueous solution undergo an unusual morphology evolution including rapid fission into small ones, swelling and final collapse of the offspring vesicles. During this process, the intrinsic fluorescence response of the vesicles allows intuitive tracking of the hierarchical structural evolution of the self-assembled membranes and straightforward quantitation of the stimuli. This work exemplifies a rational design of auto-recording stimuli-responsive nanovesicles.

Stimuli-responsive vesicles (SRVs) have attracted much research interest because of their high applicability in smart drug delivery and bio-sensing/imaging [1–4]. Because of the important physiological effects of endogenous gaseous species, a variety of nanovesicles capable of displaying significant morphologic change upon interaction with reactive sulfur (such as H_2S_n) [5,6] or reactive oxygen (such as H_2O_2 and NO) [7–13] have been developed. While sulfur dioxide (SO_2) is known as an environmental pollution gas associated with acid rain [14], endogenous SO_2 is currently regarded as a new gasotransmitter with many important physiological functions such as adjusting cardiovascular function and maintaining redox equilibrium [15–18]. SO_2 inhalation or excessive intake of SO_2 derivatives from food is associated with various diseases including cardiovascular diseases, respiratory diseases and neurological disorder [19–22]. However, SO_2 or its derivatives in aqueous solution have not been successfully employed to trigger membrane reconstitution of nanovesicles to date. Another remaining challenge in designing SRVs is to track the membrane structure evolution of the stimulated vesicles conveniently. To address these issues, reactive hydrogen-bonded (HB) skeletons and fluorescent membrane probes were integrated into self-assembled lipid membranes to construct high-performance SO_2-responsive vesicles herein reported.

Dye-interbedded vesicles (DIVs) with unique optical properties, such as porphysomes [23,24] and polydiacetylene lipid vesicles [25,26], can be formed by self-assembly of dye-derived amphiphiles. The coordination of π-stacking aggregation of the chromophores with hydrophobic interaction between the lipid chains in self-assembling usually results in the formation of uniform vesicles with relatively low critical vesicle concentrations. However, because aggregation of organic dyes generally leads to fluorescence quenching, only few examples of fluorescent DIVs had been reported and most of them employed special core dyes featured by aggregation-induced/enhanced emission [27,28]. Based on a self-assembly pattern similar to that of DIVs yet immune to compact stacking of the fluorophores in the responsive interlayers, the vesicles investigated in this work were fabricated from HB polymers bearing amphiphilic side chains and sparse fluorogenic pendants. For modular assembly of the HB polymers, both of the fluorescent subunits (AnB) and amphiphilic subunits (BOPC, BODP and BOAB) were designed to bear a barbituric acid (BA) terminal group (Scheme 1a). While each BA group contains two acceptor-donor-acceptor arrays of hydrogen-bonding sites in a coplanar manner, the melamine (Mel) linker bears three arrays of the complementary donor-acceptor-donor bonding sites. Because of the strong

* Corresponding author.
E-mail address: lishua@xmu.edu.cn (S. Li).

https://doi.org/10.1016/j.cclet.2022.02.005
1001-8417/

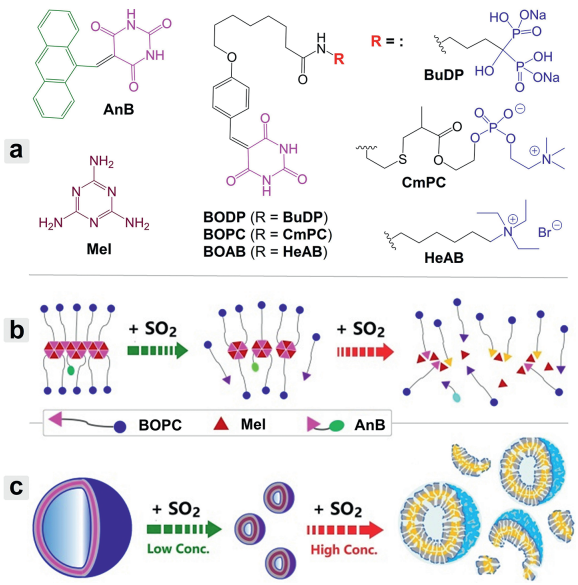

Scheme 1. (a) Chemical structures of the functional subunits investigated. Schematic illustration of (b) the SO_2-induced degradation of the HB polymers formed by AnB, Mel and BOPC, and (c) the resulting morphology change of the self-assemblies in aqueous solution.

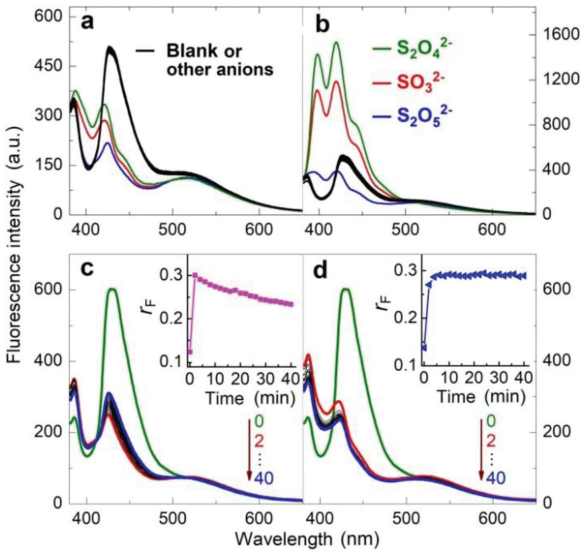

Fig. 1. (a, b) Fluorescence responses of ABMP ([AnB] = 2.0 μmol/L) in aqueous solution buffered at pH 7.0 (by 0.02 mol/L Na_2HPO_4-NaH_2PO_4) upon addition of different amount (a, 0.10 mmol/L; b, 1.0 mmol/L) of Na_2SO_3, $Na_2S_2O_5$, $Na_2S_2O_4$, $Na_2S_2O_3$, $Na_2S_2O_8$, Na_2SO_4, CH_3COONa, $NaHCO_3$, $Na_2C_2O_4$, $NaNO_2$, $NaNO_3$, NaSCN, Na_2S, NaCl and NaI, respectively. (c, d) Time dependence of the fluorescence response induced by Na_2SO_3 (c, 10 μmol/L; d, 100 μmol/L) at 25 °C. Excitation wavelength: 371 nm. Insets: plot of the emission intensity ratio (r_F, at 514 nm/422 nm) *vs.* incubation time.

hydrogen-bonding interaction between BA and Mel and high π-stacking tendency of the resulting planar HB networks [29,30], vesicular membranes with embedded fluorophores can be easily formed by co-assembly of the fluorescent subunit, amphiphilic subunits and Mel in aqueous solution.

Modularization strategy greatly facilitates rational design of the SO_2-responsive fluorescent amphiphiles. Classical aromatic fluorophores such as anthracene and pyrene have been widely employed to explore membrane structure because of their unique dual-fluorescence properties including monomer emission with structured vibronic features sensitive to the chemical microenvironment and excimer emission dependent on the aggregation state [31–34]. In designing the fluorescent subunit, anthracene was conjugated with BA to act as a membrane probe covalently immobilized on the sensory interlayer. On the other hand, the terminal BA group was proposed to be an efficient SO_2 triggering site, since the high-affinity interaction between carbonyl and bisulfite had long been known in food chemistry [35,36]. Nucleophilic addition of bisulfite onto the BA-containing subunits leads to the yield of related sulfonic acid derivatives [37,38]. The as-induced degradation of the HB networks and hydrophilicity increase of the subunits are able to drive dramatic reconstitution of the self-assembled membranes (Schemes 1b and c). Inspired by biological membrane structures, the main amphiphilic subunit was designed to bear amphoteric phosphorylcholine as the hydrophilic group. Meanwhile, two other kinds of amphiphilic subunits with anionic and cationic hydrophilic heads, respectively, were prepared for a control investigation. Importantly, the multiplicity and ratios of the functional subunits can be flexibly modulated to optimize the target-responsive performances of the co-assemblies.

The co-assembly of AnB, Mel and BOPC at a molar ratio of 1:20:29 in aqueous solution readily led to formation of a new type of fluorescent vesicles. At a typical AnB concentration of 2.0 μmol/L, the diameters of the co-assemblies (named as ABMP) formed at pH 7.0 were at the level of 300∼500 nm as revealed by dynamic light scattering (DLS) and transmission electron microscopy (TEM) studies. The regularly spherical structure of the co-assemblies was found to be readily destroyed upon treatment with low concentrations of the fungicide dodecyl-guanidine monoacetate (dodine), confirming formation of vesicular membranes but not micelles from the amphiphilic HB polymers [39–41]. Flow cytometry investigation of the solution revealed that the vesicle concentration was 2.7×10^{-14} mol/L (Fig. S10 in Supporting information). Benefiting from the biomimetic membrane surfaces, the vesicles showed a low nonspecific adsorption level in the presence of a variety of biological substances (Fig. S11 in Supporting information). Replacement of BOPC with BOAB or BODP resulted in the formation of fluorescent vesicles with structural comparability. All these vesicles can be assembled from the functional subunits at relatively low concentration levels, indicating an increased self-assembly tendency induced by participation of the π-stacking aggregation of the HB skeletons. In neutral phosphate-buffered solution, the critical vesicle concentration of ABMP in neutral phosphate-buffered solution was detected to be 12 μmol/L of the BA-bearing subunits (Fig. S12 in Supporting information). However, formation of vesicular membranes from the HB polymers was found to occur only when the molar fraction of AnB in the BA-bearing subunits was kept at a low level (<10%) (Fig. S14 in Supporting information). It is clear that coordination between π-stacking aggregation of the HB skeletons and hydrophilic-hydrophobic interaction of the amphiphilic side chains, which sustains the membranous self-assemblies in water, was greatly hindered by dense rigid pendants on the HB polymers.

The vesicular ABMP co-assemblies displayed atypical dual fluorescence from anthracene (Fig. 1) and high spectral stability in neutral aqueous solution (Fig. S15 in Supporting information). The long-wavelength signal at 514 nm was assigned to the excimer emission of anthracene, while the local (monomer) emission band appeared as an array of strongly-split double peaks (at 386 nm and 426 nm, respectively) instead of common triple peaks, indicating a high steric restriction of the fluorophores in the self-assembled membranes. Interestingly, the pH dependence of the fluorescence behavior of ABMP in the pH range 4∼9 was ignorable (Fig. S16 in Supporting information). This was mainly attributed to the protective effect of lipid membranes on the HB skeletons.

Bisulfite binding reactivity of the BA-bearing subunits was confirmed by infrared, mass and nuclear magnetic resonance spec-

tra (Figs. S17-S19 in Supporting information), and a series of SO_2-related anionic species were then tested as external stimuli for the fabricated vesicles. Addition of the SO_2-generating species resulted in remarkable fluorescence responses, while no obvious spectral changes have been observed upon addition of other species. Sharply different responses were induced by low- and high-concentration Na_2SO_3, respectively. Low-concentration stimulation suppresses the monomer emission of ABMP (Fig. 1a), while high-concentration stimulation leads to appearance of a restructured monomer emission band with clear vibrational features and enhanced intensity (Fig. 1b). These responses were found to depend on pH with an observation that the sensitivity decreased with increasing pH from 4.4 to 9.1 (Fig. S20 in Supporting information). This observation confirms that bisulfite, the distribution coefficient of which displays a same pH dependence profile, is responsible for reacting with the BA-bearing subunits because of its unique nucleophilic addition reactivity. Furthermore, the response sensitivity towards sulfite is higher than that towards pyrosulfite while lower than that towards hyposulfate, which is in tune with their SO_2/bisulfite generating ability under the testing conditions. Continuously bubbling the solution of ABMP with CO or NO gas has not induced any fluorescence response. All these observations suggest high selectivity of the stimuli-responsive system towards SO_2.

The effect of side chain structure of the amphiphilic subunits on the SO_2-responsive performance was investigated. When BOAB or BODP instead of BOPC was employed as the amphiphilic subunit, the resulting fluorescent co-assemblies were found to be less stable in aqueous solution and their SO_2 response sensitivities were obviously reduced (Fig. S21 in Supporting information). It seems that the phosphorylcholine-dominated biomimetic membrane surface is greatly helpful for stabilization of the co-assemblies. Unsurprisingly, decorating ABMP vesicles with cetyltrimethylammonium or 1-hexadecane-sulfonate also led to obvious spectral desensitization towards SO_2 (Fig. S22 in Supporting information) and the as-decorated vesicles were found to be of great degradation tendency (Fig. S23 in Supporting information).

SO_2 stimulation caused immediate fluorescence change of ABMP. Figs. 1c and d show the spectral evolutions of ABMP in reaction with sulfite at pH 7.0. Because the fluorescence responses were sectionalized, two typical concentrations of sulfite were tested. No matter the relatively high- or low-concentration stimulation induced reliable response within a couple of minutes. The rapid and sensitive response was mainly attributed to strong bisulfite affinity of the fluorescent or amphiphilic subunits where multiple nucleophilic addition sites (including the carbonyl groups of BA and the bridging methine group) are available for bisulfite (Figs. S18 and S19 in Supporting information). It should be noted that the response induced by low-concentration stimulation was retracted slightly and continuously within one hour (Fig. 1c). This unusual phenomenon is attributed to the weak self-repairing ability of the sensory co-assemblies, considering the fact that co-assembly of the subunits is a dynamic process and there are some free subunits remaining in the aqueous phase. As a contrast, no such retraction has been observed upon high-concentration stimulation which caused serious degradation of the self-assembled membranes as reflected by the germination of triple-peak monomer emission (Fig. 1d).

The fluorescence evolutions of ABMP upon increasing SO_2 stimulation were shown in Figs. 2a-d. The corresponding morphologic changes the co-assemblies were revealed by TEM images (Figs. 3a-d). Increasing addition of sulfite at relatively low concentration levels leads to the gradual reduction of the monomer emission at 426 nm while the excimer emission is kept almost unchanged (Fig. 2a). The monomer emission band remains strongly split at this stage, indicating that most of the fluorophores are still involved in compact aggregates. TEM study

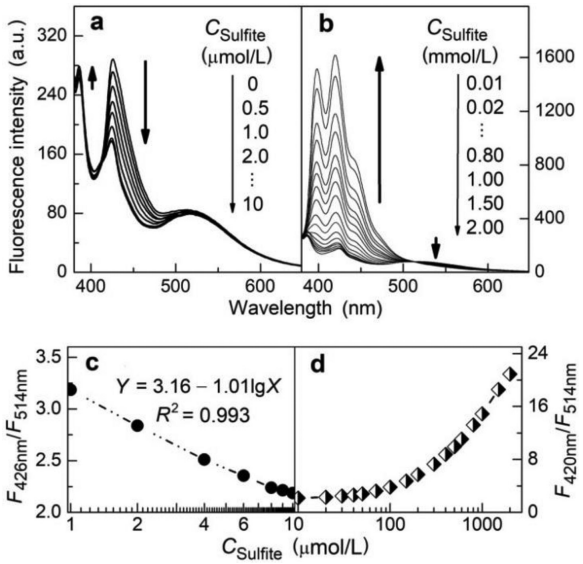

Fig. 2. Fluorescence traces (a and b, emission spectra; c and d, ratiometric responses) of ABMP ([AnB] = 2.0 μmol/L) in aqueous solution at pH 7.0 in the presence of increasing amount of Na_2SO_3. Excitation wavelength: 371 nm. Incubation conditions: 37 °C, 10 min.

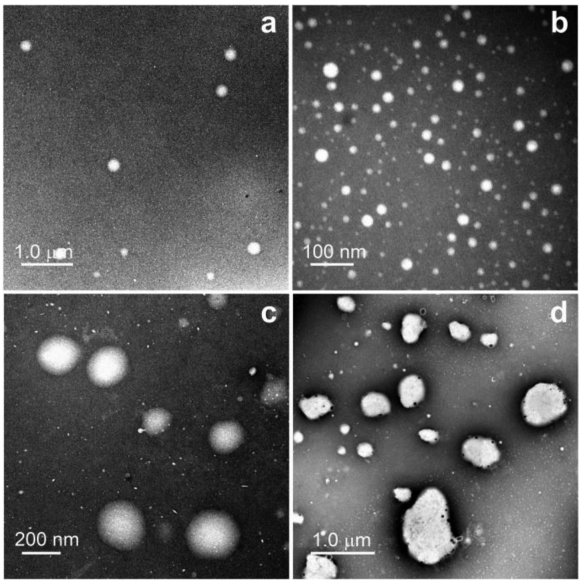

Fig. 3. TEM images of ABMP ([AnB] = 2.0 μmol/L) formed in aqueous solution buffered at pH 7.0 in the presence of different amount of Na_2SO_3: (a) none, (b) 10 μmol/L, (c) 90 μmol/L, (d) 200 μmol/L. The images were obtained *via* negative staining of the samples by 2% tungstophosphoric acid.

revealed that low-concentration SO_2 stimulation induced the fission of ABMP co-assemblies (Fig. 3a) to yield smaller vesicles (Fig. 3b), agreeing with the increased particle concentration revealed by flow cytometry (Fig. S10 in Supporting information).

Nucleophilic addition of bisulfite on the BA groups inevitably causes degradation of the HB skeletons of the co-assemblies. When only slight degradation occurs, π-π stacking of the HB-polymer fragments is still strong enough to maintain intense aggregation of these amphiphilic fragments to form self-assembled membranes, which agrees well with the unaffected excimer emission. However, only smaller vesicles with decreasing curvature radius can be formed because of the shortened HB skeletons. In addition, bisulfite capture yields sulfonic acid derivatives of the BA-bearing subunits and therefore creates a microenvironment with increasing

polarity for the fluorophores, as reflected by an enhancement in intensity of the first vibronic peak at 386 nm arising from 0-0 transition at the expense of that of the other peak of the monomer emission [33,34].

Further addition of bisulfite leads to serious degradation of the HB skeletons. Because of the increased hydrophilicity and remarkably reduced π-aggregation tendency of the degraded HB networks, the self-assembled membranes are reorganized with increasing degree of looseness. As a spectral reflection, a gradual reduction of the excimer emission is accompanied by the onset and enhancement of the typical triple-peak monomer emission of anthracene (at 398 nm, 420 nm and 445 nm, respectively) (Fig. 2b). Our analysis was also confirmed by TEM imaging of stimulated ABMP co-assemblies. As shown in Figs. 3c and d, high-concentration stimulation leads to the swelling and eventual collapse of the sensory vesicles. During this process, the hydrophilicity increase of interbedded HB networks was believed to be mainly responsible for deformation of the supramolecular vesicles. In a referential test, a metamorphosis of ABMP from vesicles to nanotubes was observed when half of the AnB subunits were substituted by violuric acid to reform the sensory co-assemblies (Fig. S24 in Supporting information). DLS tracking of the stimulated co-assemblies revealed a particle size evolution of ABMP in solution consistent with the TEM imaging results (Fig. S25 in Supporting information).

The sectionalized fluorescence response of ABMP, which indicates two different membrane degradation patterns respectively (Scheme 1c), can be utilized to establish wide-dynamic-range quantitation of the SO_2 stimulation. Because the molar ratio of the fluorophores to the reactive BA groups in ABMP is at a low level of 1/30, the fluorescence response was plotted as a function of the concentration logarithm of sulfite (lgC_T). In the low-concentration stimulation region, the monomer (at 426 nm) to excimer (at 514 nm) emission ratio decreases linearly with lgC_T (Fig. 2c). In the high-concentration region, the monomer (at 420 nm) to excimer emission ratio increases with lgC_T at an ever-accelerating pace (Fig. 2d), mainly because of the continuously-reduced amount of BA groups in the stimulated co-assemblies. It should be emphasized that the monomer emission profiles in the two regions are sharply different, although numerically there is an overlap between the monomer-to-excimer ratiometric responses in these two regions. As a reflection, ratio of the emission intensity at 426 nm to that at 409 nm is higher than 1.2 upon the low-concentration stimulation but maintains lower than 1.2 in the high-concentration region, offering a useful ancillary parameter for quantitation of the stimuli (Fig. S27 in Supporting information). Overall, fluorescent quantitation of SO_2 derivatives can be carried out with a wide dynamic range across four orders of magnitude ($10^{-7}\sim10^{-3}$ mol/L). At pH 7.0, the limit of detection was calculated to be 0.12 μmol/L. More sensitive response can be obtained at a lower pH (above 4.4). The fluorescence responses of ABMP towards SO_2 were further evaluated in the coexistence of other anionic species and found to be immune to the interference from these co-existing species in neutral aqueous solution (Fig. S28 in Supporting information).

In summary, high-performance SO_2-responsive vesicles have been facilely fabricated *via* modular self-assembly. The vesicular membranes were assembled from HB polymers consisting of a Mel-BA HB skeleton with pendant anthracene fluorophores and amphiphilic side chains. Selective capture of bisulfite in the HB networks rapidly induced membrane reconstitution of the vesicles accompanied by definable fluorescence changes. Low-concentration SO_2 stimulation caused fission of the vesicles into small ones, while high-concentration stimulation led to swelling and even collapse of the vesicles. The described two degradation patterns were recorded by efficient fluorescence responses with sharply-different emission features. The unique fluorescence responses can also be utilized to establish straightforward quantitation of the stimuli with a wide dynamic range. Our work thus exemplifies a new mode of SRVs with fluorescent auto-recording function. With triggering sites integrated into the compactly-aggregated interlayers, the self-assembled sensory membranes undergo unusual hierarchical reconstitution upon stimulation, suggesting their potential applications as self-sorting and/or sequential drug releasing nanocarriers.

Declaration of competing interest

The authors have declared no conflict of interest.

Acknowledgments

This work was supported by the National Natural Science Foundation of China (NSFC) (Nos. 21775129, 21475111), and the Foundation for Innovative Research Groups of NSFC (No. 21521004).

Supplementary materials

Supplementary material associated with this article can be found, in the online version, at doi:10.1016/j.cclet.2022.02.005.

References

[1] U. Kauscher, M.N. Holme, M. Bjornmalm, M.M. Stevens, Adv. Drug Deliv. Rev. 138 (2019) 259–275.
[2] P. Xing, Y. Zhao, Small Methods 2 (2018) 1700364.
[3] Z. Al-Ahmady, K. Kostarelos, Chem. Rev. 116 (2016) 3883–3918.
[4] A. Feng, J. Yuan, Macromol. Rapid Commun. 35 (2014) 767–779.
[5] Q. Yan, W. Sang, Chem. Sci. 7 (2016) 2100–2105.
[6] J. Zhang, X. Hao, W. Sang, Q. Yan, Small 13 (2017) 1701601.
[7] Q. Hao, Y. Kang, J. Xu, X. Zhang, Langmuir 36 (2020) 4080–4087.
[8] Z. Li, Y. Hu, Q. Fu, et al., Adv. Funct. Mater. 30 (2020) 1905758.
[9] J. Song, L. Lin, Z. Yang, et al., J. Am. Chem. Soc. 141 (2019) 8158–8170.
[10] S. Guo, S. He, Z. Chen, Y. Zhang, J. Mol. Liq. 277 (2019) 672–680.
[11] J. Zhou, Q. Tang, J. Zhong, et al., J. Mater. Sci. 53 (2018) 14063–14074.
[12] F. Zhou, B. Feng, T. Wang, et al., Adv. Funct. Mater. 27 (2017) 1703674.
[13] Z. Li, Z. Tan, A. Ding, et al., Chem. Commun. 53 (2017) 535–3538.
[14] N. Alexis, C. Barnes, I.L. Bernstein, et al., J. Allergy Clin. Immunol. 114 (2004) 1116–1123.
[15] Y. Huang, C. Tang, J. Du, H. Jin, Oxid. Med. Cell. Longev. (2016) 8961951.
[16] Z.Q. Meng, Z.H. Yang, J.L. Li, Q.X. Zhang, Chemosphere 89 (2012) 579–584.
[17] X. Wang, H. Jin, C. Tang, J. Du, Eur. J. Pharmacol. 1 (2011) 1–6.
[18] D. Liu, H. Jin, C. Tang, J. Du, Mini Rev. Med. Chem. 10 (2010) 1039–1045.
[19] F. Pannullo, D. Lee, L. Neal, et al., Environ. Health 16 (2017) 29.
[20] N. Sang, Y. Yun, H. Li, et al., Toxicol. Sci. 114 (2010) 226–236.
[21] J. Sunyer, F. Ballester, A.L. Tertre, et al., Eur. Heart J. 24 (2003) 752–760.
[22] W.L. Beeson, D.E. Abbey, S.F. Knutsen, Environ. Health Perspect. 102 (1998) 813–822.
[23] J.F. Lovell, C.S. Jin, E. Huynh, et al., Nat. Mater. 10 (2011) 324–332.
[24] K.A. Carter, S. Shao, M.I. Hoopes, et al., Nat. Commun. 5 (2014) 3546–3557.
[25] E. Lebegue, C. Farre, C. Jose, et al., Sensors 18 (2018) 599.
[26] S. Okada, S. Peng, W. Spevak, D. Charych, Acc. Chem. Res. 31 (1998) 229–239.
[27] H. Feng, J.W.Y. Lam, B.Z. Tang, Coord. Chem. Rev. 406 (2020) 213142.
[28] H. Chen, M. Li, Chin. J. Polym. Sci. 37 (2019) 352–371.
[29] J.A. Zerkowski, J.C. Macdonald, C. Seto, D.A. Wierda, G.M. Whitesides, J. Am. Chem. Soc. 116 (1994) 2382–2391.
[30] B.J. Cafferty, D.M. Fialho, J. Khanam, R. Krishnamurthy, N.V. Hud, Nat. Commun. 7 (2016) 11328.
[31] K. Kalyanasundaram, J.K. Thomas, J. Am. Chem. Soc. 99 (1977) 2039–2044.
[32] H.W. Often, W.D. Turley, J. Phys. Chem. 86 (1982) 3501–3503.
[33] P. Lianos, R. Zana, J. Phys. Chem. 84 (1980) 3339–3341.
[34] R. Humphry-Baker, M. Grätzel, Y. Moroi, Langmuir 22 (2006) 11205–11207.
[35] G.C. Whiting, R.A. Coggins, J. Sci. Food Agric. 11 (1960) 705–709.
[36] L.F. Burroughs, A.H. Sparks, J. Sci. Food Agric. 24 (1973) 187–198.
[37] Q. Zhang, Y. Huang, Y. Wang, S. Li, Y. Jiang, Dyes Pigm. 169 (2019) 111–117.
[38] X. He, W. Xu, F. Ding, et al., J. Agric. Food Chem. 68 (2020) 11774–11781.
[39] D. Lichtenberg, Biochim. Biophys. Acta 821 (1985) 470–478.
[40] J.R. Ruiz, F.M. Goñi, A. Alonso, Biochim. Biophys. Acta 937 (1988) 127–134.
[41] J.P.S. Cabral, Antimicrob. Agents Chemother. 35 (1991) 341–344.